ACS Crystal Growth and Design Manuscript Draft

Title: Attrition-enhanced deracemization of $NaClO_3$: Comparison between ultrasonic and abrasive grinding

Authors: Christos Xiouras[†], Jasper Van Aeken[†], Joris Panis[†], Joop H. Ter Horst[‡], Tom Van Gerven[†] and Georgios D. Stefanidis[†*]

† Process Engineering for Sustainable Systems (ProcESS), Department of Chemical Engineering KU Leuven, Celestijnenlaan 200F, 3001 Leuven, Belgium

‡ EPSRC Centre for Innovative Manufacturing in Continuous Manufacturing and Crystallisation (CMAC), Strathclyde Institute of Pharmacy and Biomedical Sciences (SIPBS), Technology and Innovation Centre, University of Strathclyde, 99 George Street, Glasgow G1 1RD, U.K.

[*]Correspondence to: Georgios D. Stefanidis

Tel**:** +32(0)16321007

E-mail: Georgios.Stefanidis@cit.kuleuven.be

Type of Manuscript: Article

Keywords: ultrasound; deracemization; Viedma ripening; Ostwald ripening; sodium chlorate

Abstract: Ultrasound-enhanced grinding is a more practical alternative to glass bead-enhanced grinding for performing attrition-enhanced deracemization at large scale or in continuous flow. In this work, both ultrasound-enhanced grinding (41.2 kHz) and glass bead-enhanced grinding were applied to induce Viedma deracemization of sodium chlorate ($NaClO_3$) crystals in isothermal conditions. The results demonstrate that high intensity, low frequency ultrasound can achieve efficient grinding of enantiomorphous $NaClO_3$ crystals, producing small crystal size and narrow size distribution, both being highly desirable final product properties. Monitoring the width of the crystal size distribution, reveals its crucial role and offers further insight on the underlying phenomena in the deracemization process. Compared to glass bead-enhanced grinding, ultrasound-enhanced grinding resulted in faster crystal size reduction, and rapid initial deracemization. However, further increase in the enantiomeric excess was hindered after prolonged times of ultrasonication. This ensues probably due to the absence of crystal size-induced solubility gradients, owing to the existence of close to monodispersed sized crystals after the initial stage in the ultrasound-enhanced grinding process. We show that this can be overcome by combining: a) ultrasound with glass beads, or b) ultrasound with seeding, both of which led to enantiopurity.

Attrition-enhanced deracemization of $NaClO_3$: Comparison between ultrasonic and abrasive grinding

Christos Xiouras[†], *Jasper Van Aeken*[†], *Joris Panis*[†], *Joop H. Ter Horst*[‡], *Tom Van Gerven*[†] *and Georgios D. Stefanidis*[†,*]

[†] Process Engineering for Sustainable Systems (ProcESS), Department of Chemical Engineering KU Leuven, Celestijnenlaan 200F, 3001 Leuven, Belgium

[‡] EPSRC Centre for Innovative Manufacturing in Continuous Manufacturing and Crystallisation (CMAC), Strathclyde Institute of Pharmacy and Biomedical Sciences (SIPBS), Technology and Innovation Centre, University of Strathclyde, 99 George Street, Glasgow G1 1RD, U.K.

[*]Correspondence to: Georgios D. Stefanidis

Tel: +32(0)16321007, Email: Georgios.Stefanidis@cit.kuleuven.be

KEYWORDS: ultrasound; deracemization; Viedma ripening; Ostwald ripening; sodium chlorate

ABSTRACT

Ultrasound-enhanced grinding is a more practical alternative to glass bead-enhanced grinding for performing attrition-enhanced deracemization at large scale or in continuous flow. In this work,

both ultrasound-enhanced grinding (41.2 kHz) and glass bead-enhanced grinding were applied to induce Viedma deracemization of sodium chlorate ($NaClO_3$) crystals in isothermal conditions. The results demonstrate that high intensity, low frequency ultrasound can achieve efficient grinding of enantiomorphous $NaClO_3$ crystals, producing small crystal size and narrow size distribution, both being highly desirable final product properties. Monitoring the width of the crystal size distribution, reveals its crucial role and offers further insight on the underlying phenomena in the deracemization process. Compared to glass bead-enhanced grinding, ultrasound-enhanced grinding resulted in faster crystal size reduction, and rapid initial deracemization. However, further increase in the enantiomeric excess was hindered after prolonged times of ultrasonication. This ensues probably due to the absence of crystal size-induced solubility gradients, owing to the existence of close to monodispersed sized crystals after the initial stage in the ultrasound-enhanced grinding process. We show that this can be overcome by combining: a) ultrasound with glass beads, or b) ultrasound with seeding, both of which led to enantiopurity.

1. INTRODUCTION

Enantiomers of chiral molecules are a special class of stereoisomers that can exist in non-superimposable, mirror images of one another. Most physical properties of enantiomers are identical, but their chemical behavior can be significantly different in an asymmetric environment, such as the human body[1] (*e.g.* D- isomer of dopa is toxic, while L- isomer is a precursor to dopamine, a drug used for treating Parkinson's disease[2]). This has large implications for the pharmaceutical and fine chemical industry, where most chemical syntheses of chiral drugs or chiral drug intermediates result in an equimolar mixture of the two enantiomers, known

as a racemic mixture. Currently, there is high demand in the industry for new and cost-effective processes to obtain enantiopure compounds starting from a racemic mixtures[3]. To achieve that, one can perform separation of the two enantiomers, a process termed chiral resolution. Another option is to perform deracemization, which converts the racemic mixture into a single enantiomer. Crystallization processes, being relatively simple and inexpensive, play a central role in chiral resolution at a large scale, with diastereomeric salt formation being the international state-of-the-art method[4]. However, detailed information regarding solid-liquid equilibria, extensive screening for suitable resolving agents, and precise control of the process parameters are necessary to design these processes in a robust manner[3,4].

In 2005, Viedma reported on a novel process based on attrition-enhanced deracemization, by means of grinding, which allowed for complete conversion of a racemic suspension of sodium chlorate ($NaClO_3$) crystals to an enantiopure solid phase, by rigorous stirring in the presence of glass beads[5] (Scheme 1). The practical simplicity of this process, also termed as Viedma ripening[6], has spurred great interest and since 2005 it has been extended to several other achiral molecules that crystallize as chiral crystals[7–9], but also to chiral organic molecules that crystallize as conglomerates and are readily racemizable in solution[10–12]. The method was also recently combined with a reversible reaction between achiral substrates to yield an enantiopure chiral product[13]. The total time required to reach homochirality varies greatly for different compounds, usually in the order of days, but can be decreased and steered to the desired enantiomer by introducing an initial excess (e_0) of the target enantiomer or special chiral additives. The actual mechanism of chiral symmetry breaking in a Viedma ripening process is subject of ongoing research, and is now believed to include attrition, caused by the abrasive action of the glass beads, Ostwald ripening of differently sized crystals and chirally selective agglomeration[14–16].

Understanding the interplay between these mechanisms and optimizing their action is a necessary step towards scale-up and intensification of the Viedma ripening process.

Although glass bead-enhanced grinding serves nicely in illustrating the phenomenon of attrition-enhanced deracemization, the industrial scale application of this method is cumbersome. Beads can be a source of impurities and they have to be separated from the solid product[17]. Long processing times also lead to high energy consumption. Several studies have focused on using alternative methods for optimizing or even replacing grinding in the Viedma ripening process, for example using industrial bead mill[18], spatial temperature variations[11,19] and temporal temperature variations[20,21]. Ultrasound-enhanced grinding can potentially alleviate some of the practical difficulties inherent to the glass bead-enhanced grinding, although proper design of such a system is necessary to overcome the ultrasound intensity decrease when larger volumes are involved. The implosion of cavitation bubbles in the suspension during sonication results in high velocity micro-jets and micro-turbulences, which can efficiently break down large crystals via surface erosion and inter-particle collisions, possibly accelerating deracemization[22–24]. Although the benefits of ultrasound in crystallization processes have been demonstrated, only one study investigates its effects on the deracemization process, without the addition of glass beads. Rougeot and co-workers recently showed that deracemization of a chiral organic molecule by means of ultrasonic grinding is possible, with the deracemization rate being dependent on the applied ultrasound power[25].

Herein we investigate the application of ultrasound-enhanced grinding, as an industrially more accessible alternative to glass bead-enhanced grinding, to intensify deracemization of mixtures of chiral $NaClO_3$ crystals in contact with their saturated solution. The results from comparison of the two grinding modes highlight their major differences and offer new insight into the

optimization of the Viedma ripening driving forces. A hybrid method combining the advantages of ultrasound and glass bead grinding is also presented. Further, crystal size distribution (CSD) and the effect of seeding are closely looked into and provide information on the mechanism of total chiral symmetry breaking in heterogeneous systems.

2. EXPERIMENTAL SECTION

2.1 Preparation of chirally pure $NaClO_3$ crystalline material

$NaClO_3$ powder (reagent grade, ≥ 99.0 %) was purchased from Sigma Aldrich. A re-crystallization method based on the experiments of Kondepudi et al.[26] was applied to obtain chirally pure crystalline material of both left- and right-handed crystals with a regular shape at a size of ~200 μm. 120 g of the $NaClO_3$ powder was added in a magnetically stirred, 250 mL cone flask containing 100 mL of Milli-Q water, to create a suspension at room temperature. The stirred suspension was then slowly heated to 55 °C and maintained at this constant temperature for 30 min to dissolve all crystalline material. The clear solution was then allowed to slowly cool down to room temperature, while stirring. The crystalline material was obtained using vacuum filtration of the suspension, washed, oven dried and stored in hermetically closed jars. Several samples of the resulting powder were taken and the handedness of the cubic crystals of ~200 μm was determined by means of polarized light microscopy (see Section 2.3). It was confirmed that crystals of only one handedness were present. This process was repeated in order to obtain sufficient amount of crystalline material of both chiralities for the deracemization experiments.

2.2 Deracemization experiments

2.2.1 $NaClO_3$/water suspension preparation

Different amounts of crystalline *d*-$NaClO_3$ and *l*-$NaClO_3$ were weighed, to give a known initial mass-based enantiomeric excess (20%-50%) according to: $e_0' = |m_d - m_l|/(m_d + m_l)$, where m_d and m_l are the mass of *d* and *l* crystals respectively. The total mass of *d* and *l* crystals was 6 g, constant for all experiments. The crystals of both handedness were mixed, ground together by means of pestle and mortar and placed in the respective reaction vessel, at room temperature, along with 20 mL of saturated $NaClO_3$ solution, to create a suspension of total 1.398 g/g H_2O concentration of $NaClO_3$. All experiments took place at 30 °C. At this temperature, the solubility of $NaClO_3$ is 1.031 g/g H_2O[27], which leaves ~4.6 g of $NaClO_3$ (mass of H_2O = 12.75 g) undissolved in suspension. To ensure that this initial dissolution process does not significantly affect the starting enantiomeric excess (e_0), samples were taken 5 min after attaining 30 °C, in some experiments, and e_0 was measured (see Section 2.3). In all cases, the measured number-based e_0 did not deviate significantly from the initial mass-based e_0'. All deracemization experiments were performed at least twice and standard error bars are included with the results.

2.2.2 Deracemization using glass bead-enhanced grinding

The $NaClO_3$/water suspension was placed into a 100 mL reactor vessel (internal ø 4 cm) together with 4-12 g of 3 mm glass beads (Sigma Aldrich) and an oval-shaped PTFE magnetic stirrer bar (0.5 cm x 2 cm, no ring) and the vessel was subsequently closed hermetically. The experiments were performed on IKA RH basic stirring/heating plates at 30 °C ± 2 °C and stirring speeds between 350-1750 rpm. The experiments were run for a total of 12 hours and suspension samples were taken every hour to determine the enantiomeric excess (*e*) of the crystalline phase in the suspension.

2.2.3 Deracemization using ultrasound-enhanced grinding

The $NaClO_3$/water suspension was placed into a 100 mL jacketed reactor vessel (internal ø 4 cm). A Picotest G5110A waveform generator was used to generate electric signal, which was amplified by an E&I 1020L RF power amplifier and converted to ultrasound by an ultrasonic transducer (Ultrasonics World MPI-7850D-20_40_60H). The frequency of the applied ultrasound was constant at 41.2 kHz and the power absorbed by the mixture was kept constant at 35W ± 3W in all experiments. Absorbed power was based on the power amplifier readings and was not determined calorimetrically. The experimental setup used in this work does not allow accurate determination of the mechanical energy involved in glass bead-enhanced grinding and the acoustic energy involved in ultrasound-enhanced grinding, which hampers an accurate comparison of the efficiency of the two processes. Stirring at 600 rpm was applied by a Cole Parmer overhead mixer (max. speed 2500 rpm). Due to the heating effect of ultrasound, cooling was applied by flowing water at ambient temperature through the jacket of the vessel to maintain the temperature at 30 ^{o}C ± 2 ^{o}C. The main components of the ultrasound deracemization setup can be seen in Figure S1 of the Supporting Information.

2.2.4 Deracemization using combination of ultrasound- and glass bead-enhanced grinding

These experiments were also conducted in the ultrasound deracemization setup. After 1 hour of sonication (same conditions as in the ultrasound experiments), 8 g of glass beads were added and the ultrasound irradiation was halted. After stopping the ultrasound and cooling, temperature was maintained at 30 ^{o}C ± 2 ^{o}C by means of a Philips Infrared 150R 150W lamp, since flowing water in the jacket was available only at a lower temperature.

2.3 Determination of enantiomeric excess in the crystalline phase of a suspension

Suspension samples (total of 0.1 mL) were pipetted out of the suspension, while stirring, from different locations of the vessel and placed on covered glass petri dishes (4 cm ø). Immediately after sampling, visual inspection of the crystal size and shape was performed and pictures were taken using a polarized light microscope (Olympus BX41) coupled with a Hamamatsu C4742-95 Digital Camera Controller at different magnifications. Solid phase enantiomeric excess in the same samples was determined after the crystals were left to grow for 1-2 hours, while the suspension slowly cooled down to room temperature. To ensure the absence of primary nucleation of random handedness crystals, samples with known e_0 = 100% were left to grow at the same conditions. No decrease in *e*, due to formation of new crystals of opposite handedness, was observed in these samples. The crystals were analyzed using the same polarized light microscope at 10x magnification. Starting from crossed polarizing filters (0^o), the bottom polarizing filter was rotated clockwise ($2\text{-}3^o$) to determine the optical rotatory dispersion of individual crystals. Dextrorotatory crystals change color to light blue, while levorotatory crystals appear amber, with the relative angle between the polarizing filters being the determinant factor for the color change. The number based-enantiomeric excess *e* on absolute basis was calculated based on the determined handedness of ~150-200 crystals for each sample using the equation:

$$e = \frac{|n_d - n_l|}{(n_d + n_l)} * 100$$

Where n_d and n_l are the number of *d* and *l* crystals, respectively.

3. RESULTS

3.1 Deracemization using glass-bead enhanced grinding

A first set of experiments was designed to investigate the chiral symmetry breaking of $NaClO_3$, starting from various levels of initial enantiomeric excess e_0 (20%-50%), under conditions of abrasive grinding enhanced by glass beads. All these experiments were performed under the same conditions (8 g of glass beads at 700 rpm, 20 mL, 30 °C) varying only e_0 and the results are presented in Figure 1. In every case, the solid phase spontaneously evolved towards an enantiomerically pure crystalline phase with enantiomeric excess e = 100%. The previously reported sigmoidal kinetic profiles[9,21,25] were observed here as well, being more pronounced for the experiments starting at higher e_0. The enantiomer type of crystals that was initially in excess always dominated in the end of the experiment, in accordance with previous studies[5,6]. Since no difference was observed whether starting with *d* or *l* crystals, both types were used interchangeably to create the e_0 (*e* values are reported in absolute terms). Figure 1 (left) shows that a higher e_0 will lead to complete deracemization faster. Figure 1 (right) shows that the natural logarithm representation of *e* vs time follows an approximately linear trend. The dotted lines in Figure 1 represent first order model lines for e_0= 20%-50% and $k = 0.139 \pm 0.005$ h^{-1} (k was determined by fitting all the experimental data with $e < 90\%$ to $\ln(e/e_0) = kt$). The single value of *k* for all data shows that the rate of deracemization is independent of the e_0.

The abrasive grinding of the crystals, ensured by the dispersion of the beads in the vessel, leads to ablation of small fragments from the larger crystals and to a progressive crystal size reduction, in the early stage of the process, as seen in Figure 2 (left). The size distribution of the crystals appears to be broad, with several large crystals in the 100 μm range and smaller crystals down to 30 μm. Smaller (chiral) clusters might also be present, as first postulated by Uwaha[28], responsible for the exponential enantiomeric excess increase, but their visual detection would not be possible by means of optical microscopy. A large variation of sizes is still apparent, even after

6 hours of grinding. It is likely that the observed size variations give rise to small solubility differences, as predicted by the Gibbs-Thomson rule, accelerating Ostwald ripening: the dissolution of smaller crystals that feed the larger ones[16]. Since the enantiomeric crystalline phase that is initially present in excess contains significantly more surface area, re-crystallization of the achiral solution phase or enantioselective re-incorporation of chiral clusters prior to their dissolution is likely to occur more frequently on these surfaces. On the contrary, small fragments originating from the minority enantiomeric crystalline phase are more likely to dissolve[6,28]. Continuous occurrence of this re-crystallization-growth process (Scheme 1) ultimately results in the observed *e* increase.

Both stirring speed and the amount of glass beads influence the abrasive grinding and thus the rate of deracemization. To obtain better understanding of the main parameters affecting the evolution of *e*, two new sets of experiments were performed. These started from e_0 = 30%, at the same conditions, either varying the amount of glass beads (0 g – 12 g) at constant stirring speed or the stirring speed (350 rpm - 1750 rpm) at constant amount of glass beads. The results of these experiments are shown in Figure 3 and Figure 4, respectively. Dotted lines represent first order model fits for different *k* values estimated for each series by fitting experimental data with $e < 90\%$ to $\ln(e/e_0) = kt$. At the lower stirring speed of 350 rpm and in the absence of glass beads (black curves in Figure 3 and Figure 4), *e* evolution profiles are no longer exponential but exponential curves are still fitted, based only on the increasing *e* points, in order to allow for comparison.

By increasing the amount of glass beads, the number of collisions between the beads and the crystals increases, leading to more efficient grinding. A higher amount of glass beads leads to faster deracemization, creating smaller crystals at a higher rate. When no glass beads were used

(only magnetic stirring), *e* remained approximately constant within the timespan of these experiments. This indicates that the action of the magnetic stirrer alone is insufficient to induce adequate amount of attrition of $NaClO_3$ crystals, hence increase in *e* is hindered. This is similar to a previous study where magnetic stirring in the absence of glass beads was found to cause only limited attrition and deracemization for a chiral organic compound at the higher speed of 1250 rpm[14]. It is worth noting that the use of an overhead mixer, in the absence of glass beads, also proved inefficient in deracemizing $NaClO_3$ suspensions under the same conditions.

Experimental results varying the stirring speed are shown in Figure 4. In the first few hours, the increase in *e* for the three experiments is comparable, which can be explained considering that the initial crystal size is quite large (~200 μm) and breakage may occur often enough, even at lower stirring speeds. However, as grinding progresses and crystal size is reduced, at the lower stirring speed (350 rpm), increase in *e* is less pronounced, which indicates insufficient breakage of the crystals. Increasing the stirring speed to 700 rpm, or even further to 1750 rpm, results in a fast increase in *e* throughout the process. Furthermore, the rate of *e* increase is rather similar for the stirring speeds of 700 rpm and 1750 rpm, even though the stirring speed is more than doubled. This implies that, at the conditions examined, the stirring speed of 700 rpm is already effective in dispersing the glass beads in the vessel promoting sufficient breakage of the crystals. An optimum value of stirring speed might exist, beyond which further increase will not significantly accelerate *e* evolution, in accordance with Viedma's initial observations[5]. Compared to previous studies, absolute deracemization times differ due to differences in the experimental conditions and/or the compounds used. However, the trends reported here are in close agreement with previous studies and highlight the importance of the process parameters that influence grinding intensity and attrition, which in turn drive Viedma ripening.

3.2 Deracemization using ultrasound-enhanced grinding

Increasing stirring speed and/or the amount of glass beads is a simple method to enhance grinding on lab scale; however, this might not hold at larger or even industrial scale, where separation of the beads from the crystals is not straightforward. In addition, when scaling-up batch processes, the attrition rate changes, for instance due to the change in the impellor tip velocity, which determines the frequency and energy involved with crystal-impellor collisions. To this direction, transitioning to a continuous flow system may, in some cases, prove beneficial, but such systems would be incompatible with the glass bead-enhanced grinding. Therefore, we are interested in the potential of ultrasound-enhanced grinding, as an alternative to glass bead-enhanced grinding, to intensify crystal attrition and promote fast deracemization in the absence of glass beads. Accordingly, we designed a set of experiments employing grinding by means of an ultrasonic transducer, maintaining the conditions as close as possible (600 rpm, 20 mL, 30 °C, e_0= 20%-50%) to the glass bead experiments. We opted working at a low frequency of 41.2 kHz, as such low ultrasound frequencies are known to induce more violent cavitation, which is desirable for efficient particle breakage[29,30]. The results of the ultrasound experiments are presented in Figure 5.

Typically, in all ultrasound experiments, significant increase in *e* is detected after the first hour. For experiments starting at the high e_0 of 40% and 50%, deracemization seems to progress also after the first hour, but with decreased rate, for the remainder of these experiments. However, for experiments with e_0 of 20% and 30% deracemization appears to halt after the first hour, demonstrating the attainment of a constant plateau value for *e*. Several experiments, starting from all levels of e_0 (20%-50%), were left to run more than 24 hours and samples were taken to verify whether deracemization is simply delayed or if it has actually stopped. None of these

experiments, even those starting at higher e_0, reached homochirality after approximately 24 hours, with *e* remaining approximately constant (Figure 5). Plateau values for *e* were thus observed in most ultrasound experiments, typically after 1 hour for e_0 of 20% and 30% (plateau values of ~40%), but also after 6-7 hours for e_0 of 40% and 50% (plateau values of ~80%). Although the results here do not reveal why plateau values occur later for the experiments starting at higher e_0, they do highlight that at the conditions examined, evolution to enantiopurity is indeed hampered at a certain point of the deracemization process.

Leveling of *e* in these experiments may occur due to the existence of a possible competitive mechanism to deracemization, for example ultrasound-induced primary nucleation of the counter enantiomeric solid phase. In this event, the deracemization process would be counteracted by the formation of new crystals with opposite chirality, causing decrease in *e*. If the two processes happen at a comparable rate, the apparent zero rate of deracemization, in the plateau regions, may be rationalized. In order to assess that possibility, we performed ultrasound experiments at identical conditions starting from an enantiopure solid phase. The results of these experiments revealed no decrease in *e*, indicating that no counteracting mechanism owing to ultrasound-induced primary nucleation is present. Indeed, primary nucleation is unexpected since the Viedma ripening process takes place at virtually zero supersaturation, which is also one of the main advantages of this process.

Pictures taken over the course of the grinding process for ultrasound experiments can be seen in Figure 2 (right). Ultrasound-enhanced grinding results in very fast crystal breakage leading to a significant average crystal size reduction within 2 hours. A narrow size distribution and small crystals (in the range of 30 μm) are observed for the ultrasound experiments after the first 2 hours. It is possible that the fast initial *e* amplification, observed for all ultrasound experiments

(Figure 5), is linked with the initial rapid crystal breakage. As larger crystals are broken into smaller parts, the total surface areas of both enantiomeric solid phases increase. Since one of the two enantiomeric solid phases is initially in excess, it would create, upon attrition conditions, more daughter crystals of the same chirality as the parent crystal; this can explain the large initial increase in e, which is measured on a crystal number basis in this work. Mass-based e' is also expected to increase due to the presence of ample surface for the majority crystalline phase, which allows for selective reattachment from the achiral solution phase or small chiral clusters, although its increase may initially be less pronounced. Unfortunately, accurate determination of e' is difficult in this work because $NaClO_3$ is achiral in solution; hence, only solid phase enantiomeric excess measurement techniques can be employed. As the grinding progresses further than 2 hours, the size distribution becomes close to monodisperse and the average crystal size of roughly 30 μm does not seem to change considerably (Figure 2, right). The absence of crystal size induced solubility gradients, due to the monodispersed sized crystals, may obstruct further dissolution-growth cycles that are believed to be essential for the deracemization process, leading to the observed e stagnation[6].

3.3 Comparison of glass bead-enhanced grinding and ultrasound-enhanced grinding

The observations in the experiments employing the two methods of grinding are indeed intriguing and serve to highlight their fundamental differences. The e evolution profile of the ultrasound experiments proved to be significantly different compared to the glass bead experiments. In all ultrasound experiments, substantial increase in e is detected after approximately the first hour, which is considerably more pronounced compared to most of the glass bead experiments. Quantitative comparison of the deracemization rates between these experiments is cumbersome, since ultrasound experiments do not seem to follow a distinct

exponential trend, contrary to most deracemization experiments using glass beads. The faster early *e* increase in ultrasound experiments can be explained by ultrasound being a more efficient grinding mechanism than the glass beads, at the conditions examined. Glass bead grinding only breaks off tiny fragments of a larger crystal surface due to the abrasive action, while bubble implosions created by ultrasound, due to transient cavitation, can potentially fracture a crystal into several smaller parts[23]. In principle, this effect could lead to faster initial *e* amplification as crystals are rapidly broken down and larger surface areas are created much faster. However, more research is required to elucidate whether the non-exponential initial *e* evolution is specific to the experimental conditions used in this work, or a general feature of the ultrasound-enhanced grinding due to the presence of a different deracemization mechanism compared to the Ostwald ripening-chiral cluster re-incorporation one. It should also be mentioned that under certain experimental conditions involving the presence of chiral additives[31], or temperature gradients without abrasive grinding[11], deracemization kinetics might no longer be exponential.

Nonetheless, glass bead-enhanced grinding experiments ultimately lead to enantiopurity, while this is not observed for the ultrasound-enhanced grinding experiments. A possible explanation for this observation can be postulated by closely examining the progression of the crystal size distribution throughout the two modes of grinding. Narrower size distribution and smaller crystals (right pictures in Figure 2) are observed for every ultrasound experiment. Ultrasound indeed seems to result in faster crystal breakage compared to the glass beads, which is accompanied with initial fast *e* increase. However, when ultrasonication periods are prolonged, crystal size distribution remains approximately the same throughout the grinding process, an effect that is likely to eventually cause the observed *e* stagnation. On the contrary, when glass beads are used, the size distribution is wider, as small fragments of the larger crystals detach (left

pictures in Figure 2), even though the breakage process itself is slower. Several crystals also seem to retain a relatively large size when glass beads are used, contrary to the ultrasound experiments. This size dispersion may give rise to small solubility gradients, as dictated by the Gibbs-Thomson rule, promoting Ostwald ripening or the enantioselective re-incorporation of chiral clusters, potentially increasing the deracemization rate. Similar conclusions on the importance of crystal size were drawn by Hein et al. who studied the attrition-enhanced deracemization of a chiral organic molecule by means of glass beads. In their study, a roughly 10% lower solubility was measured in slurries of larger crystals (~5 μm) compared to slurries of smaller ones (~1 μm)[16].

3.4 Improvement of the ultrasound-enhanced grinding process

In the light of these results, we postulate that the ultrasound-assisted process (and possibly any attrition-enhanced deracemization process for that matter) will eventually lead to enantiopurity provided there is a means to sustain a certain width in the crystal size distribution, allowing the existence of crystal size induced solubility gradients. However, selectively maintaining an amount of larger crystals under uniform sonication-attrition conditions is not straightforward. To alleviate this, we devised an experiment taking into account both the fast initial *e* increase in ultrasound-enhanced grinding and the broad crystal size distribution maintained through glass bead-enhanced grinding. In this "hybrid" experiment we start by sonicating for 1 hour and subsequently we stop the ultrasound and introduce glass beads for the remaining period. The results of this experiment, compared with the glass bead and ultrasound methods alone, are displayed in Figure 6. The combined method resulted in faster deracemization compared to any of the methods alone. Note that during the period of glass bead-enhanced grinding, *e* evolves similarly for the combination experiment as it does for the normal glass bead experiment. It is

indeed the positive effect of ultrasound during the first hour that leads to significant increase in the overall deracemization rate. While this method is useful to illustrate the benefit of ultrasound in the deracemization process, it is not desirable from an industrial standpoint as the glass beads are still included.

To resolve this and to design an ultrasound-enhanced process that would lead to homochirality in the absence of glass beads, we employed seeding during ultrasound-enhanced deracemization. We theorized that by introducing larger seed crystals to the system after the establishment of the monodispersed sized crystals (~2 hours), we would broaden the crystal size distribution and thus allow the deracemization process to resume. To test this idea we performed seeded experiments using ultrasound, in which we introduced 2.5 g of large seed crystals (~200 μm, e_0= 40%) after sampling of the 2nd hour. Obviously, the addition of extra mass of a particular *e* to the system has a direct effect on the total *e* in the suspension. To separate the effect of mass addition from the physical effects that result in broadening the size distribution, it was first decided to seed with a mixture of *l* and *d* crystals corresponding to e_0 = 40%. The results of these experiments are revealed in Figure 7. Just before seeding, the *e* of the system was measured to be 50%, hence the addition of 2.5 g of e_0 = 40% would in fact decrease the total *e* to approximately 46%. Remarkably, one hour after the seed addition, *e* is still measured at 50% and after two hours it increases further to 62%. Pictures of this experiment, displayed in Figure 8, show that one hour after the addition of the seeds, crystal size distribution is considerably wider compared to the ultrasound experiment without the addition of seeds. This crystal size dispersion gives rise to further ultrasound-enhanced attrition, allowing the system to overcome the stagnation in the *e* evolution; a significant *e* increase is observed over the next hours. However, after prolonged times of ultrasonication, a leveling in *e* is again observed and the attainment of homochirality is

again hindered, indicating the need of additional seeding events. We performed a second seeded experiment in which seeding was applied after the sampling of both 2nd and 5th hour (2.5 g and 4 g respectively), this time using homochiral (e_0 = 100%) seeds. The results of this experiment in comparison with the glass bead experiment at the same conditions are presented in Figure 9. One hour after the addition of the first seed, crystal number-based *e* increases by 9% less than the expected increase in mass-based e' due to the addition of enantiopure mass. The small discrepancy can be understood if one considers that the smaller number of larger seed crystals, which are not yet (fully) fragmented by the ultrasound, are not sampled to a sufficient extend. This may result in *e* measurements that underestimate the total mass-based enantiomeric excess of the system. As expected, two hours after the addition of seeds, *e* evolves with a fast rate, beyond what is dictated by the addition of enantiopure mass alone and levels at approximately *e* = 91%. Eventually, after extended periods of ultrasonication (72 hours) *e* seems to increase further, but at a very slow rate, possibly allowing the system to reach enantiopurity.

4. DISCUSSION

4.1 Approaches in ultrasound-enhanced deracemization

Firstly, a distinction should be made between this work and alternative approaches related to the enantioselective crystallization of $NaClO_3$ crystals in the presence of ultrasonic fields. Song et al. researched the cooling crystallization of $NaClO_3$ from supersaturated solutions in an ultrasonic bath with seeding and measured the enantiomeric excess close to 100%[32]. The high enantiomeric excess found in that study was rationalized by secondary nucleation induced by the ultrasound, similarly to the older work of Kondepudi et al. who demonstrated the same effects using just stirring instead of ultrasound to induce secondary nucleation[26].

In our study, secondary nucleation may well play a role, but it is obviously insufficient by itself to explain the evolution to enantiopurity, due to the initial existence of two enantiomorphous crystal populations. Instead, continuous growth and partial dissolution of the crystals, due to the size dependence of solubility, is more likely to be the dominant mechanism although more research is needed to prove that[6]. The results obtained in our work, especially with regard to the monitoring of the crystal size distribution, seem to agree with this consensus, since broader size distribution led to faster deracemization irrespective of the type of grinding employed.

Uniform ultrasonication by means of a transducer, without seeding, resulted in a narrow crystal size distribution that led to a leveling in the enantiomeric excess. This was not observed in a recent study by Rougeot et al., where it was shown that ultrasound can result in faster deracemization compared to glass beads for a chiral organic compound[25]. Besides the obvious difference in the compounds under study, completely different ultrasound equipment was used in the two studies. In their larger scale system (> 120 mL), ultrasound was delivered at a high power (up to 90W) and lower frequency (20 kHz) by means of a thin ultrasonic probe immersed in the suspension. We delivered ultrasound at lower power (35W) and higher frequency (41.2 kHz) by means of an ultrasonic transducer glued on a glass plate and attached to the bottom of the reactor. This setup was preferred over an ultrasonic probe, because we found that it avoids undesirable contamination of the reaction mixture, which was always present when ultrasonic probes were used. Under the former conditions of Rougeot et al., greater particle size reduction was achieved due to the combination of higher intensity and lower frequency ultrasound. At the same time, the larger scale of their system may have allowed the existence of local zones, where the broadness of the crystal size distribution was maintained throughout the deracemization process. In that case, faster and complete evolution to enantiopurity is expected due to enhanced

growth-dissolution, similar to our seeded experiments. Under the latter conditions of our study, uniform ultrasonication at a lower intensity and higher frequency, resulted in less particle size reduction and narrow crystal size distribution, which, in the absence of seeding, led to a leveling in the enantiomeric excess. Indeed, more experiments are needed using different types of ultrasound equipment and varying key parameters such as ultrasound frequency and intensity to reveal their effect on the attrition process and deracemization kinetics.

4.2 Industrial importance

Ultrasound-enhanced grinding is a practical (*e.g.* simple filtration is only required to get the final product) and more scalable alternative to glass bead grinding for performing attrition-enhanced deracemization. The ultrasound technology is also compatible to continuous flow systems[29]. From a production standpoint, chemical syntheses will often result in racemic mixtures that can be subsequently crystallized to enantiomorphous crystals[2]. If only one of the enantiomers is desired, attrition-enhanced deracemization and crystallization processes may also be combined. In such a system, adding homochiral seeds obtained from a previous run, or employing a product recycle stream in continuous flow systems, would be a straightforward means to alter the size distribution and steer the system to the desired enantiomer[33]. On this ground, seeding combined with ultrasound-enhanced grinding might demonstrate an effective method to achieve attrition-enhanced deracemization on industrial scale.

5. CONCLUSIONS

This study demonstrates that ultrasound can be effectively applied to the Viedma deracemization of enantiomorphous $NaClO_3$ crystals. Ultrasound-enhanced grinding induces a faster deracemization rate compared to glass bead-enhanced grinding in the initial stages of the

process. The reason for the rate increase is the rapid breakage of the larger crystals, caused by ultrasound, when a broad crystal size distribution is present. The effect of ultrasound progressively decreases with irradiation time as the crystal size distribution becomes narrower, leading to leveling of the enantiomeric excess. A broad crystal size distribution, which allows the establishment of size-induced solubility gradients, seems to be an essential prerequisite for the successful progression of the Viedma ripening process. On this ground, combination of ultrasound and seeding with larger crystals modifies the size distribution and results in a fast deracemization rate and eventually to enantiopurity.

FIGURES

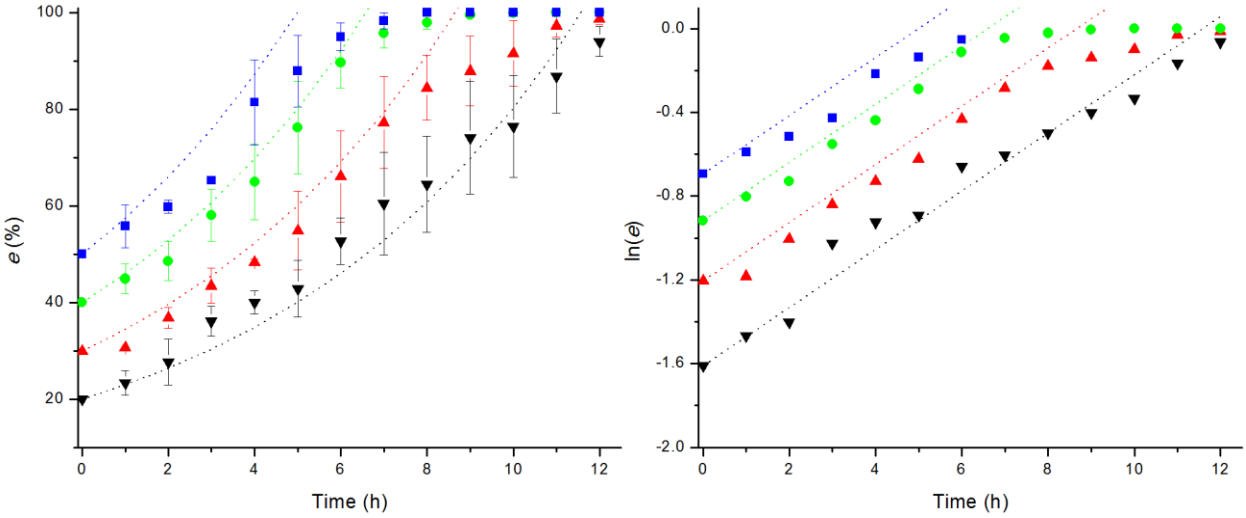

Figure 1. Left graph: Evolution of *e* in series of deracemization experiments with glass beads (8 g at 700 rpm) when starting from different initial *e*. Right graph: Evolution of ln(*e*) vs time. The experiments differ only in the starting *e*: 20% (▼), 30% (▲), 40% (●), 50% (■). Dotted curves are first order model lines for e_0=20%-50% and k = 0.139 ± 0.005 h^{-1} (k value was determined by fitting all the experimental data).

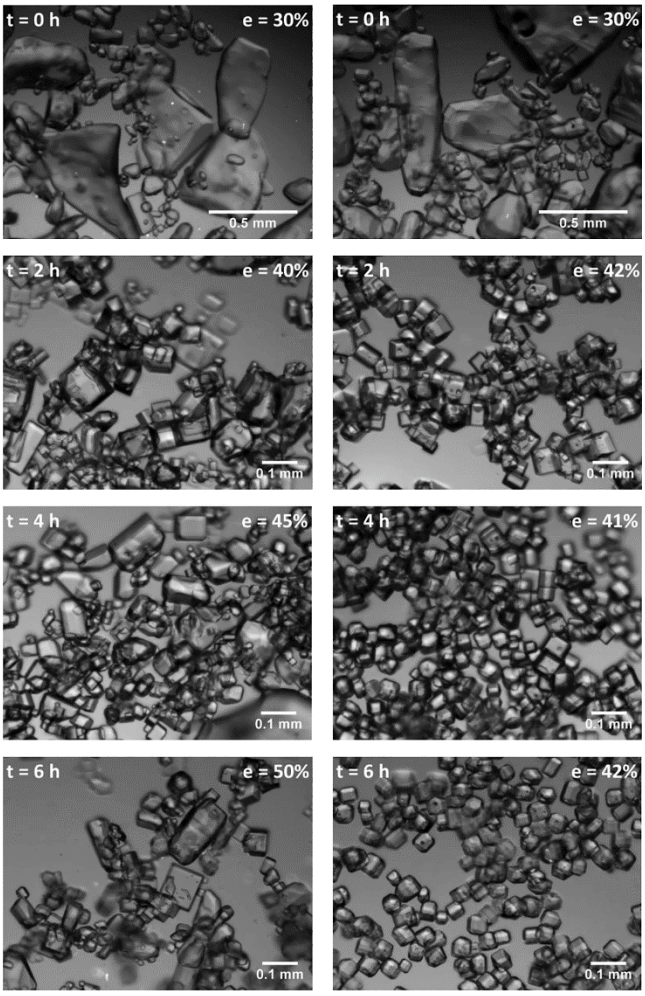

Figure 2. Comparison of crystal sizes over the course of the grinding experiments. Left: glass bead experiments (700 rpm). Right: ultrasound experiments.

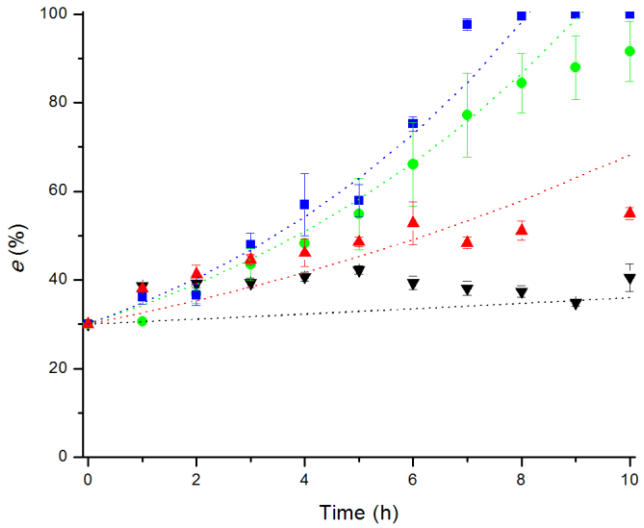

Figure 3. Evolution of *e* (stirring at 700 rpm) as a function of the amount of glass beads in grams: 12 (■), 8 (●), 4 (▲), 0 (▼). Dotted curves are first order model lines for different *k* values estimated by fitting experimental data for each series.

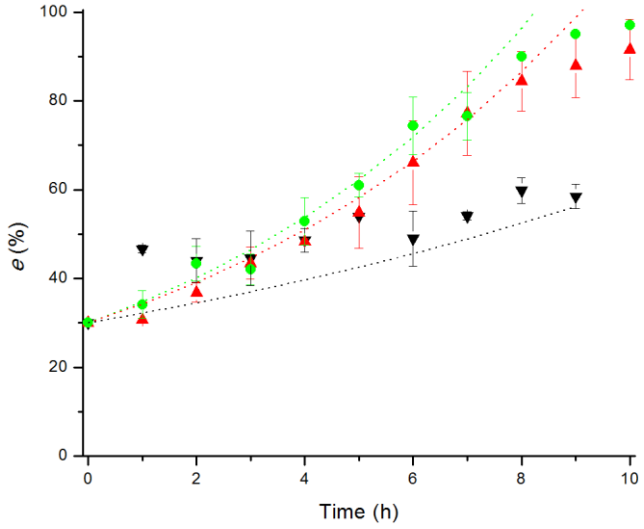

Figure 4. Evolution of *e* (8 g glass beads) as a function of magnetic stirrer revolution speed in rpm: 1750 (●), 700 (▲), 350 (▼). Dotted curves are first order model lines for different *k* values, estimated by fitting experimental data for each series.

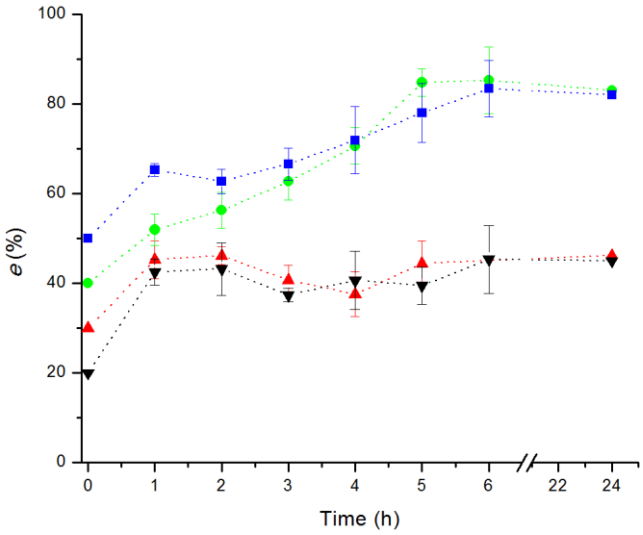

Figure 5. Evolution of *e* using ultrasound at constant temperature for different values of initial *e*. The experiments differ only in the starting *e*: 20% (▼), 30% (▲), 40% (●), 50% (■).

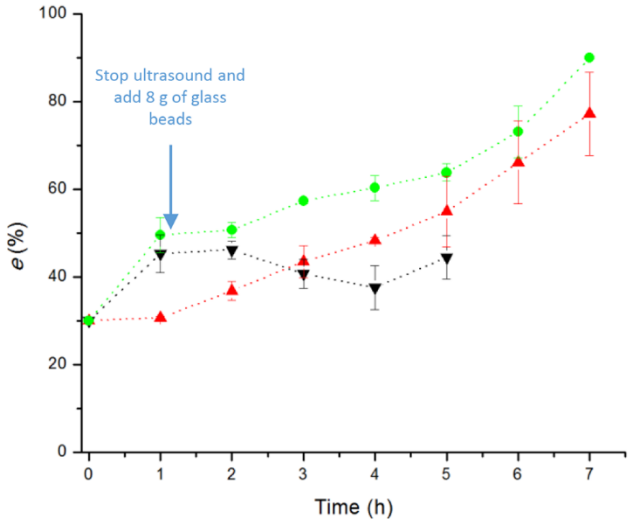

Figure 6. Evolution of *e* of ultrasound experiment (▼), glass bead (8 g, 700 rpm) experiment (▲) and combination: ultrasound for 1 h and then 8 g of glass beads (stirring at 600 rpm) without ultrasound (●).

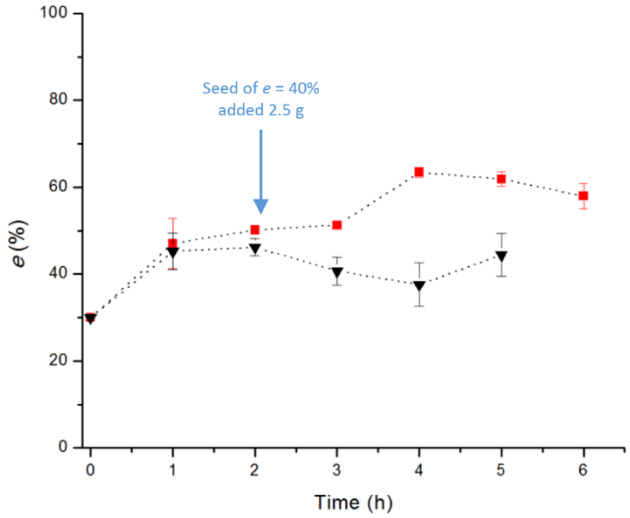

Figure 7. Evolution of *e* of the seeded ultrasound experiment (■); seeds of *e* = 40% were added after sampling at the end of the 2nd hour. Ultrasound experiments without seeding at the same conditions (▼).

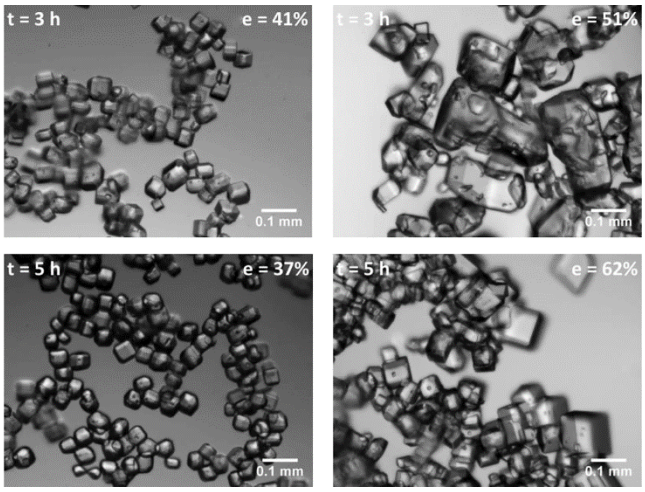

Figure 8. Comparison of crystal sizes for the ultrasound experiment (left) and the ultrasound experiment with seeding (right) at the same conditions. Seeds were added after sampling at the end of the 2nd hour. Crystal size distribution is broader in the seeded experiment, giving rise to further ultrasound-enhanced attrition and promoting Ostwald ripening; hence fast increase of *e* was observed in the next hours.

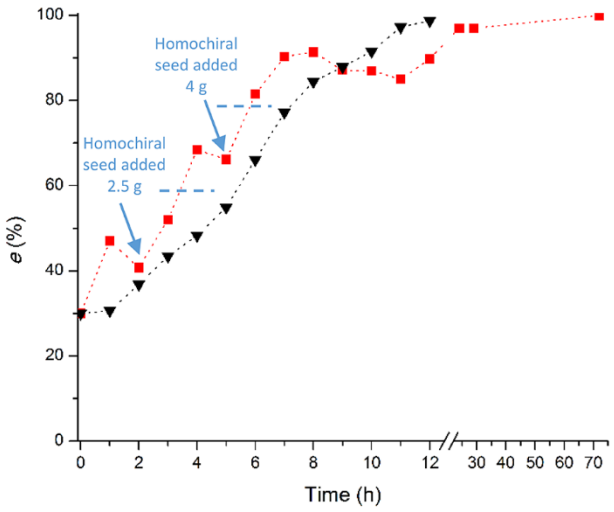

Figure 9. Evolution of *e* of the seeded ultrasound experiment (■); homochiral seeds (~200 μm) were added after sampling at the end of the 2nd and 5th hour. Dashed horizontal lines show the expected leveling of *e* only due to the addition of enantiopure mass. Glass bead experiment for comparison (▼). Error bars are omitted for visibility reasons.

SCHEMES

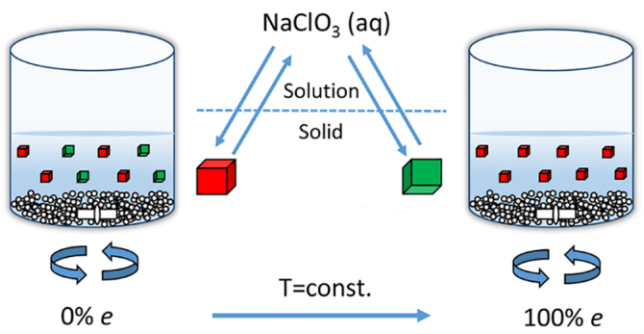

Scheme 1. Stirring a racemic mixture of chiral $NaClO_3$ crystals at constant temperature in the presence of small glass beads leads to an enantiopure crystalline phase owing to continuing mass transfer between the two crystalline phases through the solution.

ASSOCIATED CONTENT

Supporting Information

Additional description and a picture of the ultrasound setup used for the deracemization experiments. This material is available free of charge via the Internet at http://pubs.acs.org.

AUTHOR INFORMATION

Corresponding Author

* Email: Georgios.Stefanidis@cit.kuleuven.be

Author Contributions

The manuscript was written through contributions of all authors. All authors have given approval to the final version of the manuscript.

Notes

The authors declare no competing financial interest.

ACKNOWLEDGEMENT

Professor Cristóbal Viedma is thanked for his insightful answers to our questions during the progress of this work. Professor Peter Van Puyvelde and Dr. Anja Vananroye are thanked for providing the polarizing microscope.

REFERENCES

(1) Maier, N. M.; Franco, P.; Lindner, W. *J. Chromatogr. A.* **2001**, *906*, 3–33.

(2) Nguyen, L. A.; He, H.; Pham-Huy, C. *Int. J. Biomed. Sci.* **2006**, *2*, 85–100.

(3) Sheldon, R. A. *J. Chem. Technol. Biotechnol.* **1996**, *67*, 1–14.

(4) Lorenz, H.; Seidel-Morgenstern, A. *Angew. Chemie - Int. Ed.* **2014**, *53*, 1218–1250.

(5) Viedma, C. *Phys. Rev. Lett.* **2005**, *94*, 3–6.

(6) Noorduin, W. L.; Van Enckevort, W. J. P.; Meekes, H.; Kaptein, B.; Kellogg, R. M.; Tully, J. C.; McBride, J. M.; Vlieg, E. *Angew. Chemie - Int. Ed.* **2010**, *49*, 8435–8438.

(7) Viedma, C. *Astrobiology* **2007**, *7*, 312–319.

(8) Cheung, P. S. M.; Gagnon, J.; Surprenant, J.; Tao, Y.; Xu, H.; Cuccia, L. A. *Chem. Commun. (Camb).* **2008**, *8*, 987–989.

(9) McLaughlin, D. T.; Nguyen, T. P. T.; Mengnjo, L.; Bian, C.; Leung, Y. H.; Goodfellow, E.; Ramrup, P.; Woo, S.; Cuccia, L. A. *Cryst. Growth Des.* **2014**, *14*, 1067–1076.

(10) Noorduin, W. L.; Izumi, T.; Millemaggi, A.; Leeman, M.; Meekes, H.; Van Enckevort, W. J. P.; Kellogg, R. M.; Kaptein, B.; Vlieg, E.; Blackmond, D. G. *J. Am. Chem. Soc.* **2008**, *130*, 1158–1159.

(11) Viedma, C.; Ortiz, J. E.; De Torres, T.; Izumi, T.; Blackmond, D. G. *J. Am. Chem. Soc.* **2008**, *130*, 15274–15275.

(12) Steendam, R. R. E.; Brouwer, M. C. T.; Huijs, E. M. E.; Kulka, M. W.; Meekes, H.; Van Enckevort, W. J. P.; Raap, J.; Rutjes, F. P. J. T.; Vlieg, E. *Chem. - A Eur. J.* **2014**, *20*, 13527–13530.

(13) Steendam, R. R. E.; Verkade, J. M. M.; Van Benthem, T. J. B.; Meekes, H.; Van Enckevort, W. J. P.; Raap, J.; Rutjes, F. P. J. T.; Vlieg, E. *Nat. Commun.* **2014**, *5*, Article number: 5543.

(14) Noorduin, W. L.; Meekes, H.; Van Enckevort, W. J. P.; Millemaggi, A.; Leeman, M.; Kaptein, B.; Kellogg, R. M.; Vlieg, E. *Angew. Chemie - Int. Ed.* **2008**, *47*, 6445–6447.

(15) Noorduin, W. L.; Vlieg, E.; Kellogg, R. M.; Kaptein, B. *Angew. Chemie - Int. Ed.* **2009**, *48*, 9600–9606.

(16) Hein, J. E.; Huynh Cao, B.; Viedma, C.; Kellogg, R. M.; Blackmond, D. G. *J. Am. Chem. Soc.* **2012**, *134*, 12629–12636.

(17) Iggland, M.; Fernández-Ronco, M. P.; Senn, R.; Kluge, J.; Mazzotti, M. *Chem. Eng. Sci.* **2014**, *111*, 106–111.

(18) Noorduin, W. L.; Van Der Asdonk, P.; Bode, A. A. C.; Meekes, H.; Van Enckevort, W. J. P.; Vlieg, E.; Kaptein, B.; Van Der Meijden, M. W.; Kellogg, R. M.; Deroover, G. *Org. Process Res. Dev.* **2010**, *14*, 908–911.

(19) Viedma, C.; Cintas, P. *Chem. Commun.* **2011**, *47*, 12786-12788.

(20) Suwannasang, K.; Flood, A. E.; Rougeot, C.; Coquerel, G. *Cryst. Growth Des.* **2013**, *13*, 3498–3504.

(21) Steendam, R. R. E.; Van Benthem, T. J. B.; Huijs, E. M. E.; Meekes, H.; Van Enckevort, W. J. P.; Raap, J.; Rutjes, F. P. J. T.; Vlieg, E. *Cryst. Growth Des.* **2015**, *15,* 3917–3921.

(22) Zeiger, B. W.; Suslick, K. *J. Am. Chem. Soc.* **2013**, *133*, 14530–14533.

(23) Raman, V.; Abbas, A.; Zhu, W. *AIChE J.* **2011**, *57*, 2025–2035.

(24) Cintas, P. *Cryst. Growth Des.* **2008**, *8*, 2626–2627.

(25) Rougeot, C.; Guillen, F.; Plaquevent, J.-C.; Coquerel, G. *Cryst. Growth Des.* **2015**, *15*, 2151–2155

(26) Kondepudi, D. K.; Kaufman, R. J.; Singh, N. *Science* **1990**, *250*, 975–976.

(27) Chen, W.; Liu, D.; Ma, W.; Xie, A.; Fang, J. *J. Cryst. Growth* **2002**, *236*, 413–419.

(28) Uwaha, M. *J. Phys. Soc. Japan* **2004**, *73*, 2601–2603.

(29) Gielen, B.; Jordens, J.; Janssen, J.; Pfeiffer, H.; Wevers, M.; Thomassen, L. C. J.; Braeken, L.; Van Gerven, T. *Ultrason. Sonochem.* **2015**, *25*, 31–39.

(30) Jordens, J.; De Coker, N.; Gielen, B.; Van Gerven, T.; Braeken, L. *Ultrason. Sonochem.* **2015**, *26*, 64–72.

(31) Steendam, R. R. E.; Dickhout, J.; Van Enckevort, W. J. P.; Meekes, H.; Raap, J.; Rutjes, F. P. J. T.; Vlieg, E. *Cryst. Growth Des.* **2015**, *15,* 1975–1982

(32) Song, Y.; Song, Y.; Chen, W.; Chen, W.; Chen, X.; Chen, X. *Cryst. Growth Des.* **2008**, *8*, 1448–1450.

(33) Iggland, M.; Mu, R.; Mazzotti, M. **2014**. *Cryst. Growth Des.* **2014**, *14,* 2488–2493

For Table of Contents Use Only

Attrition-enhanced deracemization of $NaClO_3$: Comparison between ultrasonic and abrasive grinding

Christos Xiouras, Jasper Van Aeken, Joris Panis, Joop H. Ter Horst, Tom Van Gerven and Georgios D. Stefanidis

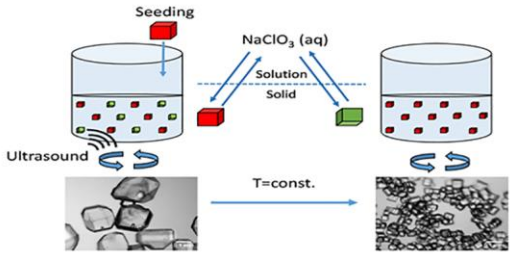

Ultrasound-enhanced grinding can replace conventional glass-bead enhanced grinding for performing Viedma deracemization. In uniform sonication-attrition conditions, the resulting crystal size distribution is narrow; hence seeding is required to maintain the crystal-size-induced solubility gradients, which seem to be decisive for fast deracemization.